$d + id'$ Chiral Superconductivity in Bilayer Silicene

Feng Liu,[1,2] Cheng-Cheng Liu,[1,3] Kehui Wu,[3] Fan Yang,[1,*] and Yugui Yao[1,3,†]

[1]School of Physics, Beijing Institute of Technology, Beijing 100081, China
[2]State Key Laboratory of Nonlinear Mechanics, Institute of Mechanics, Chinese Academy of Sciences, Beijing 100190, China
[3]Beijing National Laboratory for Condensed Matter Physics and Institute of Physics, Chinese Academy of Sciences, Beijing 100190, China

(Received 22 November 2012; published 6 August 2013)

We investigate the structure and physical properties of the undoped bilayer silicene through first-principles calculations and find the system is intrinsically metallic with sizable pocket Fermi surfaces. When realistic electron-electron interaction turns on, the system is identified as a chiral $d + id'$ topological superconductor mediated by the strong spin fluctuation on the border of the antiferromagnetic spin density wave order. Moreover, the tunable Fermi pocket area via strain makes it possible to adjust the spin density wave critical interaction strength near the real one and enables a high superconducting critical temperature.

DOI: 10.1103/PhysRevLett.111.066804 PACS numbers: 73.22.−f, 74.20.−z

Introduction.—The chiral superconductivity (SC) is a special kind of topological SC characterized by time reversal symmetry breaking [1]. In the past few years, a surge of theoretical proposals has been raised on the experimental realization of this kind of unconventional SC, including such examples as the triplet $p_x \pm ip_y$ $(p + ip')$ pairing [2,3] and the singlet $d_{x^2-y^2} \pm id_{xy}$ $(d + id')$ pairing [4–9]. While the former has probably been realized in the Sr_2RuO_4 system [10], the recent proposals [7–9] on the realization of the latter in the doped graphene system have aroused great research interests. As a result of its nontrivial topological property, the $d + id'$ pairing state will bring a series of interesting experimental consequences such as quantized boundary current [4], spontaneous magnetization [4,6], and quantized spin and thermal Hall conductance [6]. More interestingly, when realistic Rashba spin-orbital coupling is added to the system, a Majorana fermion would appear at the edge when tuning a Zeeman field [11]. While the experimental realization of this intriguing pairing state in the system may possibly suffer from such difficulty as disorders induced by doping, here we predict the realization of it in another system, i.e., the undoped bilayer silicene (BLS), which can avoid such difficulty.

Silicene, considered as the silicon-based counterpart of graphene, has attracted much attention both theoretically and experimentally [12–21]. On the one hand, similar honeycomb lattice structures of the two systems let them share most of their marvelous physical properties, especially the gapless Dirac fermions at the Brillouin-zone corner. On the other hand, due to the noncoplanar low-buckled (LB) geometry in silicene, the effective first-order spin-orbital coupling results in the quantum spin Hall effect, which can be observed in an experimentally accessible temperature regime [13]. Moreover, when the exchange field and external perpendicular electric field are added, the quantum anomalous Hall and valley polarized quantum Hall effect can be induced [15]. Just like bilayer graphene (BLG), silicene can also take the form of its bilayer version, which has recently been synthesized [18]. However, due to the LB structure of each silicene layer, there are actually more stacking ways between the two layers in the BLS than in the BLG. Therefore, it is important to study the stacking structure between the silicene bilayer and the corresponding exotic physical properties of the BLS system.

In this Letter, we first identify the optimized crystal structure and the corresponding electronic band structure of the BLS through first-principles (FP) calculations. As a result, we find that the band structure of the undoped system is intrinsically metallic with sizable Fermi pockets, whose area is tunable via strain, which opens the door to the formation of a superconducting state. Our further random-phase-approximation (RPA) based study of the system reveals that the ground state of the system is a chiral $d + id'$ pairing state, when the realistic Hubbard interaction turns on. This superconducting pairing is mediated by antiferromagnetic spin fluctuation on the border of the collinear spin density wave (SDW) order identified. Furthermore, when the SDW critical interaction strength is tuned near that of the real one via strain, the superconducting critical temperature can be high. The exotic chiral $d + id'$ SC in the BLS can thus be manipulated via strain, which opens prospects for both studying the unconventional topological SC in the new playground and for applications in silicon-based electronics.

Crystal and band structure.—The crystal and electronic band structures of the BLS reported below are obtained through our FP calculations based on the density functional theory (DFT). The electronic band structure of the system is obtained self-consistently by using the projector augmented wave pseudopotential method implemented in the

VASP package [22]. The exchange-correlation potential is treated by the Perdew-Burke-Ernzerhof potential [23].

As a consequence of the LB structure of each silicene layer, there are actually four stacking ways (see the Supplemental Material, note I [24]) between the upper and lower layers in the system. Our FP calculations reveal that two of them are stable, among which the energetically favored one (named the *AB-bt* structure) is shown in Fig. 1(a), and the corresponding phonon spectrum [25] is shown in Fig. 1(b).

From Fig. 1(a), the bottom (A_1 sublattice) of the upper silicene layer couples with the top (A_2 sublattice) of the lower layer vertically with a bond length $l_v = 2.53$ Å, while the two sublattices (A and B) within a layer couple with a bond length $l_n = 2.32$ Å. Approximately equal bond lengths, together with the bond angle $\theta = 106.60°$ between the two bonds describe an orbital hybridization more like the sp^3 type (with bond angle $\theta = 109.47°$) than the planar sp^2 type. From Fig. 1(b), the phonon frequencies obtained are real at all momenta, which suggests a stable structure. The energy of this configuration is -19.65 eV per unit cell, lower than that of the configuration studied in the literature [26], which is -19.51 eV per unit cell. It is noting here that the symmetry group of the system is D_{3d}.

The band structure of the BLS with the *AB-bt* stacking way is shown in Fig. 2(a) (left), together with its low energy zooming in (right). The most obvious feature of this band structure is the 300 meV overlap between the valence band and the conduction band, much larger than the 1.6 meV in the BLG and the 40 meV in the graphite [27,28]. Another important feature is the band crossings present not only at the K points, but also on the K-Γ axes with an energy difference between them. Such band crossings result in a three-folded symmetric pocket Fermi surface (FS) structure surrounding each K point, as shown in Fig. 2(b), where the central electron pocket is accompanied by three identical outer hole pockets with equal total area. Here, only the FS patches around one K point are present. The other patches can be obtained by six-folded rotations around the Γ point, as required by the D_{3d} symmetry and the time reversal invariant of the system.

To proceed, we construct the following effective four-band tight-binding (TB) model in the basis $\{|B_1\rangle, |B_2\rangle, |A_1\rangle, |A_2\rangle\}$, which well captures all the low energy features of the above band structure near the FS [compared with FP results in Fig. 2(a)],

$$H(\mathbf{k}) = \begin{pmatrix} \Delta & t_3 f(\mathbf{k}) & t_n f(\mathbf{k})^* & -t_2 f(\mathbf{k})^* \\ t_3 f(\mathbf{k})^* & \Delta & -t_2 f(\mathbf{k}) & t_n f(\mathbf{k}) \\ t_n f(\mathbf{k}) & -t_2 f(\mathbf{k})^* & 0 & t \\ -t_2 f(\mathbf{k}) & t_n f(\mathbf{k})^* & t & 0 \end{pmatrix}. \tag{1}$$

Here, A_i, B_i $(i = 1, 2)$ represent the basis mainly composed of the $3p_z$ orbitals localized around each of the four silicon atoms within a unit cell. The hopping integrals t_n, t, t_2, and t_3 between each two orbitals are marked in Fig. 1(a). The phase factor $f(\mathbf{k})$ is $\sum_\alpha e^{i\mathbf{k}\cdot\mathbf{R}_\alpha}$, with $\mathbf{R}_\alpha$ $(\alpha = 1, 2, 3)$ to be the nearest-neighbor vector. Finally, notice the small effective on-site energy difference Δ between the A and B atoms. The fitted parameters of the system in comparison with those of the BLG are listed in Ref. [29], from which the most obvious feature of the BLS lies in the dominating role of the vertical interlayer hopping t. The resulting strong bonding-antibonding energy split between the A_1 and A_2 orbitals pushes them far away from the Fermi level, leaving the B_1 and B_2 orbitals to form a low energy subspace which takes responsibility for the main physics of the system.

It is important to point out here that the low energy band structure of the system is considerably sensitive to biaxial strains. As shown in Fig. 4(a), for small strains which keep the symmetry and FS topology of the system, the total area of the electron or hole pockets feels a considerable variation. This tunable property of the band structure turns out to be very important for our following discussions.

Model and free susceptibility.—Let us consider the following four-band Hubbard-model of the system:

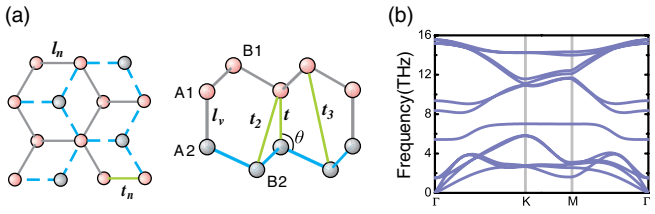

FIG. 1 (color online). (a) Optimized geometry of the BLS. (b) The corresponding phonon spectrum. In (a), both the top view (left) and side view (right) are shown. The vertical bond length l_v, the intralayer nearest neighbor bond length l_n, and the angle θ between them are marked, together with the hopping integrals between each two of the four atoms A_i, B_i $(i = 1, 2)$ within a unit cell.

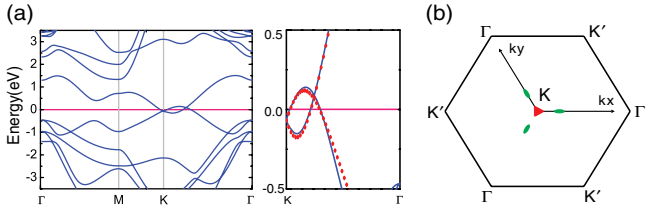

FIG. 2 (color online). (a) The band structure of BLS corresponding to the optimized lattice structure shown in Fig. 1(a). (b) The FS patches around the K point. In (a), the zooming in low energy band (right) is also shown, where the tight-binding (TB) model (red scatters) is compared with the FP results (blue solid line). In (b), the central pocket (red) is electronlike and the outer three identical pockets (green) are holelike, with the total areas of the two kinds of pockets equal.

$$H = \sum_{\mathbf{k}\sigma,\alpha\beta} c^{\dagger}_{\mathbf{k}\alpha\sigma} H_{\alpha\beta}(\mathbf{k}) c_{\mathbf{k}\beta\sigma} + U \sum_{i,\alpha=1,4} n_{i\alpha\uparrow} n_{i\alpha\downarrow}, \quad (2)$$

where $H(\mathbf{k})$ is defined by Eq. (1), i and α (β) denote the unit cell and orbital indices, respectively. Noticing that the electron-electron interaction has been included in the mean-field level in our DFT calculation, the explicit inclusion of the Hubbard repulsion here would lead to a slight renormalization of the TB parameters. However, such a slight parameter renormalization would not qualitatively change the main physics here.

The free susceptibility $\chi^{(0)l_1,l_2}_{l_3,l_4}(\mathbf{q}, i\omega_n)$ (for $U = 0$) of the model is given in the Supplemental Material, note II [24], and the $\mathbf{k}$-dependent static susceptibility of the system defined by the largest eigenvalue of the susceptibility matrix $\chi^{(0)}_{l,m}(\mathbf{q}) \equiv \chi^{(0)l,l}_{m,m}(\mathbf{q}, i\nu = 0)$ is shown in Fig. 3(a), which displays a distribution centering around the Γ point. Note that the susceptibility peak at the Γ point only suggests the same repeating pattern from one unit cell to another and within one single unit cell there can be antiferromagnetic structure, as introduced below.

SDW and SC.—When the Hubbard interaction turns on, the standard multiorbital RPA [30–32] (see also the Supplemental Material, note II [24]) approach is adopted in our study. The spin [$\chi^{(s)}$] or charge [$\chi^{(c)}$] susceptibilities in the RPA level are defined in the Supplemental Material, note II [24], and it is clear that the repulsive Hubbard interaction suppresses $\chi^{(c)}$ (hence, charge density wave instability) and enhances $\chi^{(s)}$ (hence, SDW instability). When the interaction strength U is enhanced to a critical value U_c, the spin susceptibility of the model diverges, which implies the instability toward long-range SDW order. The ordered spin structure of this bilayer system determined by the eigenvector of the spin susceptibility matrix $\chi^{(s)}_{l,m}(\mathbf{q}) \equiv \chi^{(s)l,l}_{m,m}(\mathbf{q}, i\nu = 0)$ corresponding to its largest eigenvalue is shown in Fig. 3(b), from which one finds an antiferromagnetic state with antiparallelly aligned spin patterns within a unit cell. The ordered moments are mainly distributed on the B_i ($i = 1, 2$) atoms which take responsibility for the low

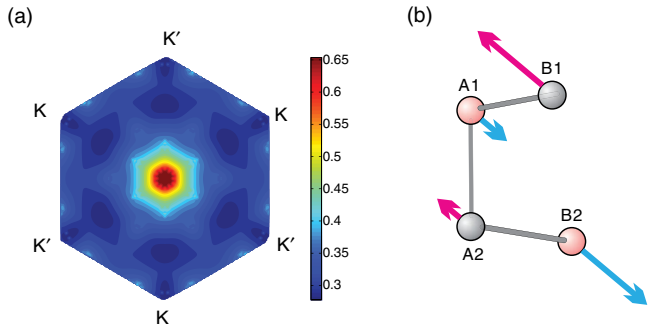

FIG. 3 (color online). (a) $\mathbf{k}$ dependence of the free static susceptibility. (b) The SDW ordered spin pattern within a unit cell.

energy physics of the system. It is noting here that with the enhancement of the strain and hence the Fermi pocket area, the SDW critical value U_c feels an obvious variation from the 1.48 eV at zero strain to the 1.18 eV at the strain of 0.06. Such a range is probably realizable for the Hubbard U of the $3p_z$ orbitals of the silicon atoms.

When the Hubbard U is near but lower than U_c, the antiferromagnetic spin fluctuation is strong in the system. Through exchanging such antiferromagnetic spin fluctuations between each Cooper pair, unconventional chiral $d + id'$ SC emerges in the BLS system.

The effective interaction obtained in the RPA level generated through exchanging spin susceptibility is $V_{\text{eff}} = \sum_{\alpha\beta,\mathbf{k}\mathbf{k}'} V^{\alpha\beta}(\mathbf{k},\mathbf{k}') c^{\dagger}_{\alpha}(\mathbf{k}) c^{\dagger}_{\alpha}(-\mathbf{k}) c_{\beta}(-\mathbf{k}') c_{\beta}(\mathbf{k}')$ (see the Supplemental Material, note II [24]), from which one obtains the following linearized gap equation [32] near T_c,

$$-\frac{1}{(2\pi)^2} \sum_{\beta} \oint_{FS} dk'_{\parallel} \frac{V^{\alpha\beta}(\mathbf{k},\mathbf{k}')}{v^{\beta}_F(\mathbf{k}')} \Delta_{\beta}(\mathbf{k}') = \lambda \Delta_{\alpha}(\mathbf{k}). \quad (3)$$

Here, the integration is along the βth FS patch. The $v^{\beta}_F(\mathbf{k}')$ is the Fermi velocity, and $k'_{\parallel}$ represents the component along the FS. Diagonalizing this eigenvalue problem, one obtains the largest eigenvalue λ, which is related to the T_c of the system through $T_c = 1.13\hbar\omega_D e^{-1/\lambda}$, and the corresponding eigenvector $\Delta_{\alpha}(\mathbf{k})$ which determines the leading pairing symmetry of the system. Here, $\hbar\omega_D$ is a typical energy scale for the spin fluctuation approximated as the low energy bandwidth, i.e., $\hbar\omega_D \approx 300$ meV.

Our RPA calculations on the BLS identify exactly degenerate d_{xy} and $d_{x^2-y^2}$ doublets as the leading pairing symmetries of the system for $U < U_c$ at all strain values, which is robust against small doping (see the Supplemental Material, note III [24]), as can be induced by the supporting substrate [33]. Both symmetries are singlet with nodal gap functions. While the $d_{x^2-y^2}$ shown in Fig. 4(c) is antisymmetric about the axis $x = \pm y$ in the reciprocal space, the d_{xy} shown in the Supplemental Material, note III [24] is symmetric about them. The two gap functions form a 2D E_g representation of the D_{3d} point group of the system. For both symmetries, two gap nodes are present on each Fermi pocket.

Since the two d-wave pairing symmetries are degenerate here in the quadratic level of the Ginsberg-Landau free energy, they would generally be superposed [9] as $\Delta(\mathbf{k}) = \Delta_1 \Delta_{d_{x^2-y^2}}(\mathbf{k}) + \Delta_2 \Delta_{d_{xy}}(\mathbf{k})$ to further lower the energy up to higher levels. Our energy optimization on the effective Hamiltonian $H_{\text{eff}} = H_{\text{band}} + V_{\text{eff}}$ yields $\Delta_2 = i\Delta_1$, which just leads to the long-sought nodeless chiral $d + id'$ SC. This superposition manner between the two d-wave symmetries satisfies the requirement that the gap nodes should avoid the FS to lower the energy. With intrinsically complex gap function, this pairing breaks time reversal

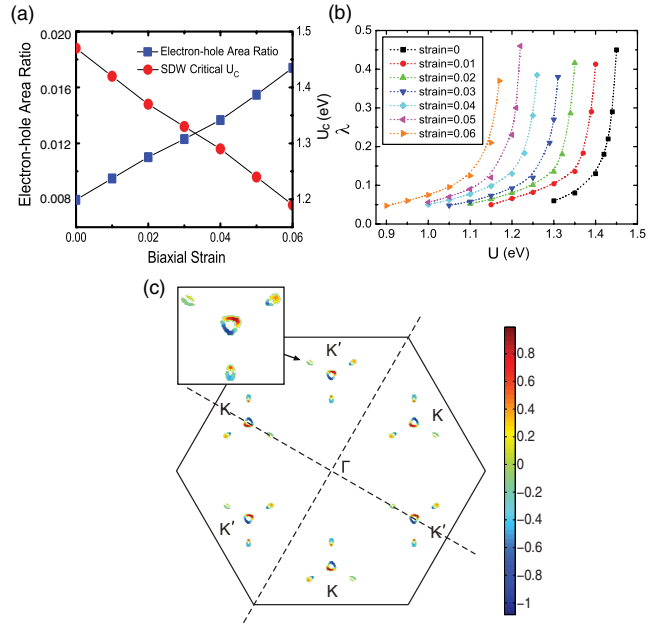

FIG. 4 (color online). (a) The biaxial strain dependence of Fermi pocket area ratio viz. the ratio of the total area of the electron and hole pockets against the total area of the Brillouin zone and the SDW critical value U_c of the BLS. (b) The interaction strength U dependence of the largest eigenvalue λ of the linearized gap function (3), which is related to T_c through $T_c = 1.13\hbar\omega_D e^{-1/\lambda}$. Results for different strain values are compared. (c) $\mathbf{k}$ dependence of the gap function of the $d_{x^2-y^2}$ symmetry for $U = 1$ eV, which is antisymmetric about the axes $x = \pm y$ shown in the reciprocal space. Inset: zooming in the vicinity of K'.

symmetry and will bring a lot of exotic properties. It is a singlet analogy of the extensively studied $p + ip'$ SC.

The U dependence of the eigenvalue λ of Eq. (3), which is related to T_c, is shown in Fig. 4(b) for different strains. Clearly, T_c increases with the Hubbard U and rises promptly at $U/U_c \lesssim 1$ as a result of the strongly enhanced antiferromagnetic spin fluctuation near the critical point. Since U_c is tunable via strain, as shown in Fig. 4(a), the ratio U/U_c varies within a range which provides basis for the realization of the relation $U/U_c \lesssim 1$ which is crucial for the high T_c of the system. For example, for $\lambda \approx 0.3$ attainable by different strains shown in Fig. 4(b), the T_c obtained can be as high as 80 K, although it is usually overestimated in the RPA level. For real material, whether high T_c can be acquired is determined by how near U/U_c can be tuned to 1.

Our RPA calculations for the system also identify a possible nodeless f-wave pairing to be the leading symmetry in the triplet channel, consistent with Ref. [34]. This pairing also breaks time reversal symmetry and the gap function changes sign with every 60° rotation, which belongs to the A_{1u} representation of D_{3d} (see the Supplemental Material, note III [24]). However, its T_c is much lower than that of the $d + id'$ pairing. Note that there are also discussions on the competition among various superconducting symmetries in graphene [35].

The $d + id'$ pairing symmetry obtained here is reliable, as it is based on the weak coupling RPA approach. As for the superconducting critical temperature T_c, the RPA approach generally overestimates T_c near the critical point. Thus, the T_c in real material might be lower than that estimated here. How to calculate the T_c accurately remains an open question. What is more, the coexistence between the SDW order and SC is also possible in the system, which is beyond the present framework. Furthermore, other types of many-body ordered states discussed in the BLG [36] are also possible here. Further studies are needed for such purposes.

Conclusion.—We have performed a FP calculation on the BLS. Through energy optimization, we identified a D_{3d} symmetric stacking structure for the system. The band structure corresponding to this crystal structure was intrinsically metallic, with Fermi pockets around each K point whose areas were tunable via strain. Further RPA-based studies predicted a chiral $d + id'$ superconducting ground state of the system for realistic electron-electron interactions. The superconducting critical temperature of this spin-fluctuation mediated SC was well tunable via strain, which could be high when the SDW critical interaction strength was tuned near that of the real one. The realization of the chiral $d + id'$ SC in the BLS predicted here will not only provide a new playground for the study of the topological SC, but also bring a new epoch to the familiar Si industry.

We are grateful to Dung-Hai Lee, Jun-Ren Shi, Fa Wang, and Hong Yao for stimulating discussions. The work is supported by the MOST Project of China (Grants No. 2014CB920903, No. 2011CBA00100) and the NSF of China (Grants No. 10974231, No. 11174337, No. 11274041, and No. 11225418). F. Y. is supported by the NCET program under Grant No. NCET-12-0038. F. L. and C.-C. L. contributed equally to this work.

*yangfan_blg@bit.edu.cn
†ygyao@bit.edu.cn

[1] M. Sigrist and K. Ueda, Rev. Mod. Phys. **63**, 239 (1991).
[2] L. Fu and C. L. Kane, Phys. Rev. Lett. **100**, 096407 (2008); X.-L. Qi, T. L. Hughes, S. Raghu, and S.-C. Zhang, Phys. Rev. Lett. **102**, 187001 (2009).
[3] M. Cheng, K. Sun, V. Galitski, and S. Das Sarma, Phys. Rev. B **81**, 024504 (2010); I. Serban, B. Béri, A. R. Akhmerov, and C. W. J. Beenakker, Phys. Rev. Lett. **104**, 147001 (2010).
[4] R. B. Laughlin, Phys. Rev. Lett. **80**, 5188 (1998).
[5] M. Vojta, Y. Zhang, and S. Sachdev, Phys. Rev. Lett. **85**, 4940 (2000).
[6] B. Horovitz and A. Golub, Phys. Rev. B **68**, 214503 (2003).

[7] A. M. Black-Schaffer and S. Doniach, Phys. Rev. B **75**, 134512 (2007); J. González, Phys. Rev. B **78**, 205431 (2008); S. Pathak, V. B. Shenoy, and G. Baskaran, Phys. Rev. B **81**, 085431 (2010).

[8] M. L. Kiesel, C. Platt, W. Hanke, D. A. Abanin, and R. Thomale, Phys. Rev. B **86**, 020507 (2012); W.-S. Wang, Y.-Y. Xiang, Q.-H. Wang, F. Wang, F. Yang, and D.-H. Lee, Phys. Rev. B **85**, 035414 (2012).

[9] R. Nandkishore, L. S. Levitov, and A. V. Chubukov, Nat. Phys. **8**, 158 (2012).

[10] A. P. Mackenzie and Y. Maeno, Rev. Mod. Phys. **75**, 657 (2003).

[11] A. M. Black-Schaffer, Phys. Rev. Lett. **109**, 197001 (2012).

[12] G. G. Guzmán-Verri and L. C. Lew Yan Voon, Phys. Rev. B **76**, 075131 (2007).

[13] C.-C. Liu, W. Feng, and Y. Yao, Phys. Rev. Lett. **107**, 076802 (2011); C.-C. Liu, H. Jiang, and Y. Yao, Phys. Rev. B **84**, 195430 (2011).

[14] S. Cahangirov, M. Topsakal, E. Aktürk, H. Sahin, and S. Ciraci, Phys. Rev. Lett. **102**, 236804 (2009); N. D. Drummond, V. Zólyomi, and V. I. Fal'ko, Phys. Rev. B **85**, 075423 (2012); Z. Ni, Q. Liu, K. Tang, J. Zheng, J. Zhou, R. Qin, Z. Gao, D. Yu, and J. Lu, Nano Lett. **12**, 113 (2012).

[15] M. Ezawa, Phys. Rev. Lett. **109**, 055502 (2012); M. Ezawa, New J. Phys. **14**, 033003 (2012); M. Tahir and U. Schwingenschlögl, Sci. Rep. **3**, 1075 (2013).

[16] M. Ezawa, J. Phys. Soc. Jpn. **81**, 104713 (2012).

[17] B. Lalmi, H. Oughaddou, H. Enriquez, A. Kara, S. Vizzini, B. Ealet, and B. Aufray, Appl. Phys. Lett. **97**, 223109 (2010); L. Chen, C.-C. Liu, B. Feng, X. He, P. Cheng, Z. Ding, S. Meng, Y. Yao, and K. Wu, Phys. Rev. Lett. **109**, 056804 (2012).

[18] B. Feng, Z. Ding, S. Meng, Y. Yao, X. He, P. Cheng, L. Chen, and K. Wu, Nano Lett. **12**, 3507 (2012).

[19] P. Vogt, P. De Padova, C. Quaresima, J. Avila, E. Frantzeskakis, M. C. Asensio, A. Resta, B. Ealet, and G. Le Lay, Phys. Rev. Lett. **108**, 155501 (2012).

[20] A. Fleurence, R. Friedlein, T. Ozaki, H. Kawai, Y. Wang, and Y. Yamada-Takamura, Phys. Rev. Lett. **108**, 245501 (2012).

[21] A. Kara, H. Enriquez, A. P. Seitsonen, L. L. Y. Voon, S. Vizzini, B. Aufray, and H. Oughaddou, Surf. Sci. Rep. **67**, 1 (2012).

[22] G. Kresse and J. Furthmüller, Phys. Rev. B **54**, 11169 (1996).

[23] J. P. Perdew, K. Burke, and M. Ernzerhof, Phys. Rev. Lett. **77**, 3865 (1996).

[24] See Supplemental Material http://link.aps.org/supplemental/10.1103/PhysRevLett.111.066804 for details, where electronic properties and structure optimization for four possible stacking configurations are given in note I; the RPA approach and the pairing symmetries details can be found in note II and III.

[25] A. Togo, F. Oba, and I. Tanaka, Phys. Rev. B **78**, 134106 (2008).

[26] T. Morishita, S. P. Russo, I. K. Snook, M. J. S. Spencer, K. Nishio, and M. Mikami, Phys. Rev. B **82**, 045419 (2010).

[27] E. McCann and V. I. Fal'ko, Phys. Rev. Lett. **96**, 086805 (2006).

[28] B. Partoens and F. M. Peeters, Phys. Rev. B **74**, 075404 (2006).

[29] TB parameters fitted for the BLS in comparison with those of the BLG [28] are given below: t_n, t, t_2, t_3, and Δ for *AB-bt* (BLG) are 1.13 (3.12), 2.025 (0.377), 0.15 (0.12), 0.62 (0.29), and -0.0691 (-0.0366) eV, respectively.

[30] T. Takimoto, T. Hotta, and K. Ueda, Phys. Rev. B **69**, 104504 (2004).

[31] K. Yada and H. Kontani, J. Phys. Soc. Jpn. **74**, 2161 (2005); K. Kubo, Phys. Rev. B **75**, 224509 (2007); I. I. Mazin, D. J. Singh, M. D. Johannes, and M. H. Du, Phys. Rev. Lett. **101**, 057003 (2008); K. Kuroki, S. Onari, R. Arita, H. Usui, Y. Tanaka, H. Kontani, and H. Aoki, Phys. Rev. Lett. **101**, 087004 (2008).

[32] S. Graser, T. A. Maier, P. J. Hirschfeld, and D. J. Scalapino, New J. Phys. **11**, 025016 (2009).

[33] G. Profeta, M. Calandra, and F. Mauri, Nat. Phys. **8**, 131 (2012); B. Uchoa, and A. H. Castro Neto, Phys. Rev. Lett. **98**, 146801 (2007).

[34] B. Roy, arXiv:1211.1748.

[35] F. M. D. Pellegrino, G. G. N. Angilella, and R. Pucci, Eur. Phys. J. B **76**, 469 (2010).

[36] O. Vafek, Phys. Rev. B **82**, 205106 (2010); V. Cvetkovic, R. E. Throckmorton, and O. Vafek, Phys. Rev. B **86**, 075467 (2012).